Paper No.
02504

CORROSION 2002

A COMPACT APPARATUS FOR TESTING EROSION-CORROSION UNDER DISTURBED FLOW CONDITIONS CONSISTING OF A ROTATING CYLINDER WITH A STEP

Srdjan Nesic*, Jeremy Bienkowsky, Andrew Purchase*, Klaus Bremhorst,

Department of Mechanical Engineering, The University of Queensland, Brisbane, Qld 4072, Australia

and

Kyung-Soo Yang, Jong-Yeon Hwang

Department of Mechanical Engineering, Inha University, 253 Yonghyun-Dong,

Nam-ku, Inchon, 402-751,

Republic of Korea

ABSTRACT

Erosion-corrosion is most severe in the vicinity of flow disturbances. In the past, erosion-corrosion under disturbed flow conditions has been studied experimentally in flow loops and numerically by performing flow simulations. In this study a new, compact experimental setup was tested, intended for study of erosion-corrosion under disturbed flow conditions, involving a rotating cylinder geometry with a sudden step.

A thorough characterization of this new setup was initiated, involving wall mass transfer measurements complemented with Direct Numerical Simulation of the turbulent flow around it. A large variation of the wall mass transfer rates behind the step was measured similar in character to the one obtained in flow through a sudden pipe expansion. Flow simulations have confirmed that this flow geometry will create a qualitatively similar mean flow pattern as observed in a sudden pipe expansion flow involving flow separation and reattachment. The simulations have also shown that there is a large-scale unsteadiness in the turbulent flow structure downstream the step, a fact that might have a significant impact on erosion-corrosion.

---

* Current address: NSF I/U CRC Corrosion and Multiphase Flow, Ohio University, Stocker Center, Athens, OH, USA.

INTRODUCTION

Single-phase flow affects corrosion in a number of ways. When bare metal surfaces corrode, the effect of flow is manifested through altered mass transfer of species involved in the corrosion reaction. When surface films are present in corrosion, flow can contribute to their removal either through dissolution (which is often under mass transfer control) or by mechanical erosion. There are many overlapping terms for this type of corrosion, the most common term being erosion-corrosion, which will be used in the present work.

It is a well-established fact that erosion-corrosion is most severe in the vicinity of flow disturbances. Flow disturbances such as sudden steps, protrusions, bends, etc., give rise to complex flow patterns with increased turbulence levels, mass transfer and surface stresses.

In the past, erosion-corrosion under disturbed flow conditions has been studied experimentally in flow loops[1] and numerically by performing flow simulations[2]. Experimental studies, while expensive to conduct, offered an insight into the causes of erosion-corrosion. Numerical simulations of the flow (typically using k-ε turbulent flow simulators) were instrumental in the search for links between flow parameters and corrosion. After many arguments, the majority opinion is nowadays that high turbulence levels in the vicinity of corroding surfaces contribute to increased erosion-corrosion rates[3]. In the process of getting to this conclusion, many other concepts were tested, such as: break-away velocity[4], critical Reynolds number[5], mean wall shear stress[6], etc., but generally failed. On the other hand, the concept of "near wall turbulence" affecting corrosion still needs clarification and effective means of prediction.

In the present study a new, compact experimental setup is proposed for study of erosion-corrosion under disturbed flow conditions, involving a rotating cylinder geometry with a sudden step (see Figure 1b and Figure 2). The authors believe that this geometry can become an effective tool for studying erosion-corrosion under disturbed flow conditions and substitute much more complex and expensive flow loop based systems.

As the present paper relates to a pilot study, a thorough characterization of the stepped rotating cylinder electrode was initiated and reported below, involving wall mass transfer measurements complemented with Direct Numerical Simulation (DNS) of the turbulent flow around the electrode.

EXPERIMENTAL

The electrode

In the past, the standard rotating cylinder electrode system has often been used in electrochemical[7], mass transfer[8, 9] and corrosion[10] testing. In most cases the inner cylinder was rotating, however in some cases the measurements involved axial flow or a rotating outer cylinder. In the present investigation we have studied only the geometry comprising of a rotating inner cylinder contained within a concentric stationary outer wall. Two variations of the rotating cylinder setup were used in this project. They were:

- A standard Rotating Cylinder Electrode (RCE) consisting of a nickel cylinder mounted on a shaft (Figure 1a). The standard RCE system was used to verify that the experimental system behaved in accordance with previously established empirical correlations such as that for mass transfer[11];

- A Stepped Rotating Cylinder Electrode (SRCE) comprising of a standard RCE flow geometry and a sleeve used to produce disturbed flow (Figure 1b) and a Ø0.7 mm circular platinum patch mounted behind the step. This system was used to investigate the local mass transfer rates arising from disturbed flow behind the step.

Although for the purposes of the present investigation only one step was required on the SRCE for data acquisition, two steps symmetric with respect to the center of rotation were installed, which allowed the cylinder to be mechanically balanced at all rotational speeds (see cross-section presented in Figure 2). The rotating shaft was made from stainless steel covered by a base cylinder and a stepped sleeve both manufactured from a polymer material. The cylinder was mounted in a rotator capable of giving accurately controlled rotating speeds up to 10,000 rpm.

When rotated anti-clockwise, the rotating cylinder and sleeve arrangement forces flow separation to occur at the step. As a result of this flow separation, it was expected that reattachment and recirculation would occur behind the step. The sleeve was designed so that the distance between the base of the step and the platinum patch in the SRCE could be varied. By changing the relative position of the sleeve to the patch between data acquisition runs, it was possible to obtain mass transfer measurements behind the step throughout the entire flow-disturbed region. The step height of 2 mm was several orders of magnitudes greater than the diffusion sublayer thickness which is important if enhanced mass transfer behavior is to be observed in the turbulent flow regime.[12]

Mass transfer measurements

Experimental setup and procedures. A three-electrode electrochemical cell was used to make mass transfer measurements. (Figure 3). A saturated Ag/AgCl reference electrode was used to provide the reference potential. In order to minimize the Ohmic drop through the solution, a Luggin capillary was used. The porous wooden tip of the Luggin capillary was placed approximately 3-4 mm from the rotating cylinder during data acquisition. The Luggin capillary contained saturated KCl. The counter electrode consisted of a 80 mm diameter ring manufactured from Ø0.7 mm platinum wire which was placed concentrically around the rotating cylinder.

A potentiostat was used for measurement and control of potential and current during the experiments. An analytical speed controller was used for controlling the rotation speed of the rotating cylinder which was double-checked by using a stroboscope. Graphite carbon brushes impregnated with silver were used on the motor assembly to electrically connect the probe on the rotating cylinder.

Two different electrode reactions were tested for mass transfer measurements: oxygen reduction and potassium ferri/ferro cyanide reduction/oxidation. The latter was found to have significantly better repeatability and all mass transfer results reported here are obtained using that electrolyte. It consisted of a deaearated equimolar aqueous solution of ferri and ferro cyanide (ranging between 0.01 and 0.1 molar in different experiments) and 0.1 - 0.5 molar of potassium hydroxide which was added as a supporting electrolyte. The ferri/ferro cyanide redox reaction can be represented by:

$$Fe(CN)_6^{3-} + e^- \underset{anode}{\overset{cathode}{\rightleftharpoons}} Fe(CN)_6^{4-} \qquad (1)$$

While this reaction is known to afford good reproducibility in different flow geometries[8, 11], certain precautions must be taken. Three potential problems can arise with the usage of the ferri/ferro cyanide system:

- slow decomposition of the potassium ferro cyanide from exposure to daylight;
- poisoning of the working electrode and counter electrode as a result of hydrogen cyanide formation from the above mentioned decomposition, and
- presence of a considerable amount of oxygen in the cell, which would interfere with the above electrochemical reactions, particularly at low concentrations.

While the exact rate of decomposition of these cyanide complexes has not been quantified in the literature, Eisenberg et al.[11] suggested that it could be "practically eliminated if the electrolyte was an alkaline solution and kept in darkness", which was found to work reasonably well. Purging with nitrogen practically eliminated oxygen from the solution.

A typical preliminary experiment involved a sweep of the potential 0.5 V above and 1.7 V below the open circuit potential (E_{oc}) at 5 mV/s. In Figure 4 two representative potentiodynamic sweeps using SRCE are shown, taken at a rotational speed of 2000 rpm (Re=38,600). The two experiments were done under identical conditions in the same solution and were separated 5 days, during which the solution was stored in the dark. From Figure 4 it is clear that the cathodic reaction offers a broader potential "window" where the limiting current is clearly measurable (nearly 1 V wide) when compared to the anodic reaction (200-300 mV wide). On the other hand a lack of reproducibility of the cathodic reaction (in magnitude) was observed probably due to the slow decomposition of the ferro cyanide ion in the presence of light occurring most likely as:

$$Fe(CN)_6^{4-} + 2H_2O \rightarrow Fe(CN)_5H_2O^{3-} + OH^- + HCN \qquad (2)$$

Conversely the limiting currents associated with the anodic reaction were clearly more reproducible and they were used in all experiments reported below. Since a potentiostatic technique was employed there, the potential was fixed in the middle of the anodic diffusion limiting current region. The invariance of this potential window was checked before and after each series of potentiostatic measurements.

Validation of the mass transfer measurement technique using the rotating cylinder electrode. Before the stepped rotating cylinder was tested for mass transfer, preliminary experiments were performed to verify the accuracy of the measurement technique by comparison with published data. For fully developed turbulent flow around a standard rotating cylinder electrode, the mass transfer correlation of Eisenberg et al.[11] is a frequently used benchmark:

$$Sh = 0.0791\,Re^{0.7}\,Sc^{0.356} \qquad (3)$$

where $Sh=k_m d/D$ is the Sherwood number, k_m is the mass transfer coefficient in m/s, D is the diffusion coefficient in m^2/s, d is the cylinder diameter in m, $Re=u_0 d/\nu$ is the Reynolds number, u_0 is the cylinder peripheral velocity in m/s, ν is kinematic viscosity in m^2/s, $Sc=\nu/D$ is the Schmidt number.

A cylindrical nickel electrode was used, 12 mm in diameter and 8 mm in length (see Figure 1a). A dilute working solution (0.01 molar solution of both potassium ferri and ferro cyanide, 0.1 molar potassium hydroxide) was selected due to the relatively large surface area of the working electrode.

Newman[7] reports that the diffusivity of the ferri cyanide ion at infinite dilution in water at 25°C is 8.96×10^{-10} m^2/s. The temperature correction for the diffusivity can be found by using the Stokes-Einstein equation:

$$D = D_{ref} \times \frac{T}{T_{ref}} \times \frac{\mu}{\mu_{ref}} \tag{4}$$

where D_{ref} and μ_{ref} are the fluid properties at the reference temperature of T_{ref} =25°C. For 22°C which was the solution/room temperature during the experiments it can be found that D=8.67× 10^{-10} m^2/s, μ=1.1078 x 10^{-3} kg m/s, ρ=1020 kg/m^3, leading to a Schmidt number Sc=1224.

To select an appropriate potential range from which to evaluate the limiting currents, using a potentiostatic technique on a RCE, several sample potentiodynamic scans were taken to observe how the position of the anodic diffusion limiting current region varied with the rotational speed, as shown in Figure 5. It can be seen that the anodic diffusion limiting current region is clearly identifiable for all rotational speeds used. It was therefore decided to use the simple mean of the data points between +0.50 V and +0.51 V with respect to E_{ref} inclusively (totaling 11 data points for each curve) to evaluate the anodic diffusion limiting current.

The measured limiting currents were converted into a mass transfer coefficient:

$$k_m = \frac{I_{\lim}}{n_e F A_e C_b} \tag{5}$$

where I_{lim} is the limiting current in A, n_e is the number of mols of electrons involved in oxidising/reducing a mol of active species in mol_e/mol, F is the Faraday's constant in C/mol_e, A_e is the working electrode active area in m^2, C_b is the concentration of active species in mol/m^3.

In order to maintain generality the results were subsequently nondimensionalised and compared to the correlation of Eisenberg et al. [11] in Figure 6. The error bars shown on the plots indicate a 95% window of uncertainty for the parameters indicated on the axes. For details of the error analysis see the original work of Bienkowsky[13]. The transitional Reynolds number for flow around a rotating cylinder is 200, which corresponds to a rotational speed of approximately 30 rpm. All measurements were therefore conducted under turbulent flow conditions.

The results indicate that the measured limiting currents i.e. mass transfer rate measurements, correlated well with those predicted by using the Eisenberg et al. [11] equation. Furthermore, the repeatability of the measurements taken in different occasions and the linearity of the dimensionless plot are highlighted by the correlation coefficient, which is 0.999. It should be remarked that the present measurements were slightly higher than those predicted by the Eisenberg et al. [11] equation. The magnitude of this difference is of the same order or smaller then the experimental error in the original experiments of Eisenberg et al. [11] and is therefore considered acceptable.

Calibration of the patch electrode. In order to measure the local rates of mass transfer behind the step a small measuring probe in the streamwise direction was used. Therefore in these experiments the stepped rotating patch electrode was used as shown in Figure 1b inset. Since this active platinum patch was so small (Ø0.7 mm in diameter) it was clear that fully developed mass transfer boundary layer would not be reached in the same way as it is on long electrodes or on a standard RCE, which can be seen as an

infinitely long electrode. Therefore the small patch electrode had to be calibrated before each experiment, without the step, in order to obtain a reference value. A higher concentration of ferro/ferri cyanide (0.1 molar) was used in order to obtain measurable currents on such as small electrode.

A potentiostatic technique was used. A similar procedure was used as described for the standard RCE above. The anodic potential window was first identified using potentiodynamic measurements before each series of potentiostatic measurements. A potential of 0.62 V vs. E_{ref} was selected as a middle of this window and maintained in the potentiostatic measurements. The rotational speed was varied between 100 and 3500 rpm what corresponds to limiting currents of 100 μA and 740 μA respectively. For each velocity the potential stabilized within a few seconds and subsequently the final value of the limiting current was taken as an average of 100 points.

The results are plotted in Figure 7 for two series of measurements. The integrated turbulent Leveque equation suggested by Linton and Sherwood[14] predicts a Reynolds number dependence on the mass transfer rate of $Re^{0.583}$ for a developing concentration boundary layer, which is supported by Van Shaw et al. [15] who showed that the turbulent convective controlled mass transfer rate for a developing boundary layer should depend on $Re^{0.58}$. The experimental results support this as points are clustered around a straight line in a log-log plot with a correlation coefficient of 0.9955. The experimentally determined exponent for the Reynolds number dependence of the mass transfer rate was 0.5734 what is in good agreement with the correlation suggested by Linton and Sherwood.[14] However in a subsequent calibration the experimental slope was 0.4968 which highlighted the need for frequent calibrations. The results of these measurements were used as a basis to compare the increase in the mass transfer rate due the presence of the step.

Results of measurement of local mass transfer rates behind the step. The anodic diffusion limiting currents were measured at discrete locations behind the rearward facing step at 100, 145, 200, 500 and 1000 rpm corresponding to Reynolds numbers of 1930, 2800, 3860, 9650 and 19300 respectively based on the cylinder diameter. The measured mass transfer rates were normalized with the reference values obtained without the step (as shown in Figure 7) in order to obtain the, here-called, *mass transfer enhancement factor* due to the disturbed flow geometry. The result for the range of Reynolds number studied is plotted in Figure 8.

The most remarkable feature seen is the large variation of the mass transfer rates behind the step. The minimum value is approximately 3 to 4 times smaller while the maximum is 20% larger then the values obtained on a RCE without the step. These results are similar to the variation obtained downstream a sudden pipe expansion as reported by Sydberger and Lotz.[16] The peak value is located between 2 and 3 step heights downstream of the step and seems to move closer to the step as the Reynolds number is increased. The peak is relatively broad and there appears to be an inflexion in the curve somewhere between 4 and 5 step heights downstream the step. While common wisdom and some previous flow simulations[3] suggests that the peak in the mass transfer rate should be in the vicinity of the reattachment point this could be clarified only by accurate flow measurements and/or simulations. Due to the size and shape of the flow geometry, detailed measurements of the flow parameters downstream the step are practically impossible, therefore flow simulations were undertaken and are reported below.

Formulation

In this study, computations were carried out with respect to a reference frame rotating with a constant angular velocity (Ω). The governing incompressible continuity and momentum equations are:

$$\nabla \bullet \boldsymbol{u} = 0 \tag{6}$$

$$\frac{\partial \boldsymbol{u}}{\partial t} + (\boldsymbol{u} \bullet \nabla)\boldsymbol{u} = -\frac{1}{\rho}\nabla P + \nu\nabla^2 \boldsymbol{u} - 2\Omega \times \boldsymbol{u} \tag{7}$$

where $\boldsymbol{u}$, ρ, and ν denote velocity vector relative to the rotating reference frame, density, and kinematic viscosity, respectively. The last term in equation (8) represents the Coriolis force. Since the centripetal force is conservative, it is included in the pressure term, and does not affect the velocity field[17]. Thus, P in (8) includes not only pressure but also the centripetal potential.

The governing equations were discretized using a finite-volume method in a generalized coordinate system. Spatial discretization was second-order accurate. A hybrid scheme was used for time advancement; nonlinear terms and cross diffusion terms were explicitly advanced by a third-order Runge-Kutta scheme, and the other terms were implicitly advanced by the Crank-Nicolson method. A Fractional Step Method [18] was employed to decouple the continuity and momentum equations. For the details of the numerical algorithm used in the code, see the original reference[18].

Choice of Numerical Parameters

Simulation of the flow around SRCE was performed for Re=2800. The shape of the cylinder cross-section was taken exactly the same as that employed in the experiments. The axial (spanwise) direction was assumed as homogeneous. The outer boundary of the computational domain was located approximately 3 diameters (0.07 m) away from the center of rotation, and the axial size of the domain was approximately one diameter (0.024 m). The computational grid employed in this study is shown in Figure 9. Figure 9(a) exhibits the whole computational domain at one cross-section in the axial direction, and Figure 9(b) is a magnified view of the grid close to the cylinder. Since the cross-section geometry is symmetric with respect to the center of rotation, only one half of the cross-section was considered in the simulations. The grid is a body-fitted O-grid system, which is the most suitable type of grid for this complicated geometry, with more resolution near the steps and solid boundaries. The number of grid points was progressively refined up to 224×128×80 (in the tangential, radial, and axial directions respectively). One typical run including statistical evaluation took about 12,000 time steps which corresponds to 10 revolutions of the cylinder. One time step took approximately 50 seconds of computations on a CRAY C90 supercomputer.

Initial and Boundary Conditions

With respect to the rotating reference frame, the inner cylinder is stationary while the outer circular boundary is rotating in the clockwise direction. The initial flow field was constructed such that at any location in the flow field, the velocity was given as Ω times the distance between the point and the center of rotation (where Ω is the cylinder rotational speed in rad/s). This is an obvious choice because in the experiments the cylinder started rotating in stationary surroundings. In addition, a small-amplitude

random noise (with a root-mean-squared magnitude approximately 0.1% of the tangential speed of the cylinder surface) was added only at the beginning of the simulation in order to bypass transitional regime and to establish a self-sustaining turbulence as quickly as possible.

The no-slip boundary condition was applied on the solid surfaces and a periodic boundary condition was employed both in the tangential direction and in the axial direction. The outer boundary condition needed special attention. It seems most natural to impose a constant tangential speed of Ωr_0, where r_0 is the outer radius of the domain, on the outer boundary. This corresponds to a practical situation where the outer solid boundary is located far way from the cylinder so that the fluid there is not disturbed by the motion of the cylinder. From the numerical point of view, this solution requires a large computational domain with a fine resolution near the outer boundary, which is not the region of our interest. This would result in a significant waste of computational resources. To minimize such a waste, a "slip" boundary condition was devised and employed on the outer boundary:

$$\frac{\partial u_\theta}{\partial n} = \Omega \qquad u_r = 0 \qquad \frac{\partial u_z}{\partial n} = 0 \tag{8}$$

where u_θ, u_r, and u_z represent the tangential, radial, and axial velocity components, respectively, and n denotes the direction locally perpendicular to the outer boundary (radial direction). This boundary condition allowed use of a reasonably small computational domain without significant disturbance of the flow field near the cylinder which is the region of our primary interest. Furthermore, since in this scheme the tangential velocity gradient is exactly specified at the boundary, rather than computed during the simulation, a fine numerical resolution was not required near the outer boundary, which led to additional saving in computational time.

Results and Discussion

After the simulated flow pattern reached a statistically steady state, collecting of hydrodynamic data for statistical evaluation was initiated. Averaging of the flow field parameters was carried out in the homogeneous axial direction and also in time. More than 120 data sets were collected over 3 revolutions of the cylinder.

The mean velocity vector plot (averaged both in time and in the axial direction) in the vicinity of the step is shown in Figure 10. The main recirculating region and a secondary one near the corner can be clearly identified. A corresponding plot of the streamlines is shown in Figure 11. These two graphs confirm the original expectation that this flow geometry will create a qualitatively similar flow pattern as observed in a sudden pipe expansion or a plane backward facing step, including flow separation and reattachment.

It should be mentioned that the transient flow simulations performed in the present work have shown that there is a large scale unsteadiness in the turbulent flow structure downstream the step not seen in time averaged Figure 10 and 13. For example the position of the instantaneous reattachment "point" fluctuates significantly - up to approximately three step heights - $3h$. This is a fact that was completely missed by all the standard k-ε turbulent flow simulations reported previously for similar flow geometries (for example see Nesic and Postlethwaite[2]). To illustrate this important point, the images of the instantaneous flow pattern at the same axial plane but at two different times, approximately 0.58 revolutions apart, is shown in Figure 12. The flow patterns seen there are quite different as one can expect in turbulent flows. Similar behavior was reported by Le et al.[19] in the case of plane backward

facing step flow. This large scale unsteadiness of the flow pattern downstream the step can explain the relatively broad ("smeared") peaks in mass transfer measurements shown in Figure 8.

The distributions of the mean (time averaged) tangential wall-shear stress, $\bar{\tau}$, the fluctuating component (rms of its fluctuation), τ_{rms} and the sum of the two (total wall-shear stress), $\sqrt{\bar{\tau}^2+\tau_{rms}^2}$ downstream the step are shown in Figure 13 (the overbar represents time and space averaging in the axial direction). All the values were averaged in time and in the axial direction and normalized with $\frac{1}{2}\rho U_\theta^2$ and with the maximum value for easier comparison). One can notice that the mean reattachment point of the main recirculating region where the wall-shear stress is zero is located 4.9h downstream from the step. The largest mean wall-shear stress occurs in the recirculating region at 2.9h downstream from the step. Another interesting feature is that the rms of the wall-shear stress fluctuation is actually larger than the mean value throughout the domain. While the profile of the mean wall-shear stress bears little resemblance to the mass transfer profile, the rms profile and even more so the total wall-shear stress profile are remarkably similar to the measured mass transfer profile.

The mean total turbulence intensity is also shown in Figure 13. It was computed as $\sqrt{\left(\overline{u_i' u'}_i\right)/3}$ where u'_i denotes velocity fluctuation in each direction (Einstein summation is assumed for repeated indices). The values taken at 0.006h away from the wall were normalized with the cylinder peripheral tangential velocity U_θ as the characteristic velocity scale and with the maximum value. One can identify that a local maximum of the total turbulence intensity is found to be one step height upstream from the mean reattachment point (at 3.9h downstream from the step). This is in contrast with the previous reports that the two coincide in the case of flow through the sudden pipe expansion.[2, 3]

CONCLUSIONS

- A new, compact experimental setup was tested intended for study of erosion-corrosion under disturbed flow conditions, involving a rotating cylinder geometry with a sudden step.

- In this pilot study, a thorough characterization of the stepped rotating cylinder electrode was initiated, involving mass transfer measurements complemented with Direct Numerical Simulation of the turbulent flow around the new electrode.

- A large variation of the mass transfer rates behind the step was measured similar in character to the one obtained in flow through a sudden pipe expansion.

- Flow simulations have confirmed that this flow geometry will create a qualitatively similar mean flow pattern as observed in a sudden pipe expansion or a plane backward facing step flow.

- Further, the simulations have shown that there is a large scale unsteadiness in the turbulent flow structure downstream of the step, a fact completely missed by all the standard k-ε turbulent flow simulations reported previously for similar flow geometries, which might a have significant impact on erosion-corrosion.

- The predicted total (mean + fluctuating) wall-shear stress variation was remarkably similar to the measured mass transfer profile behind the step indicating a strong link between the two.

- Further work on characterization of the new electrode involving erosion-corrosion measurements, numerical analysis of the complex flow structure and the effect it has on erosion-corrosion, are in progress. The authors believe that in the near future, this flow geometry will become an effective tool for studying erosion-corrosion under disturbed flow conditions, and will in many cases substitute much more complex and expensive flow loop based systems.

ACKNOWLEDGMENT

The experimental study reported here was supported in part by an Australian Research Council grant. Their help is greatly appreciated. The computational part of the research was financially supported by 1998 CRAY R&D Research Fund in Korea and by a grant from The University of Queensland. Computations in the present work were carried out by using the CRAY C90 of the KORDIC supercomputer center in Korea, which is gratefully acknowledged. The help of Tuck Hoon Dave Liong in collecting some of the experimental data is appreciated.

REFERENCES

1. Lotz U. and J. Postlethwaite, "Erosion Corrosion in Disturbed Two-Phase Liquid/Particle Flow", Corrosion Science, 30, p. 95, 1990.

2. Nesic, S. and J. Postlethwaite, "Relationship Between the Structure of Disturbed Flow and Erosion-Corrosion", Corrosion J., 46, p. 874, 1990.

3. Nesic, S. and J. Postlethwaite, "Hydrodynamics of Disturbed Flow and Erosion-Corrosion, Part I, Single-Phase Flow Study", Can. J. Chemical Engineering, 69, p.698, 1991.

4. Dawson J. L. and C.C. Shih, "Corrosion under Flowing Conditions-An Overview and Model", Paper 2 in *Flow Induced Corrosion*, eds K. J. Kennelly, R. H. Hausler, D. C. Silverman, NACE, Houston, TX, 1991.

5. Mahato, B. K., S. K. Voora and L. W. Shemilt, "Steel Pipe Corrosion Under Flow Conditions, I. An Isothermal Correlation for a Mass Transfer Model", Corrosion. Science, 8, p.173, 1968.

6. Efird, K. D., "Effect of Fluid Dynamics on the Corrosion of Copper-Base Alloys in Sea Water", Corrosion J., 33, p.3, 1977.

7. Newman, J.S., "Electrochemical Systems, Second Edition", Prentice Hall, Englewood Cliffs, New Jersey, 1991.

8. Gabe, D. R., "The Rotating Cylinder Electrode", Journal of Applied Electrochemistry, 4, p. 91, 1974.

9. Gabe, D. R. and Walsh, F. C. "The Rotating Cylinder Electrode: A Review of Development", Journal of Applied Electrochemistry, Vol. 13, p. 3, 1983.

10. Silverman, D. C., "Rotating Cylinder Electrode - An Approach for Predicting Velocity Sensitive Corrosion", Corrosion/90, paper no. 13, (Houston, TX: NACE International, 1990).

11. Eisenberg, M, Tobias, C. W. and Wilke, C. R., "Ionic Mass Transfer and Concentration Polarisation at Rotating Electrodes", Journal of the Electrochemical Society, 101, p. 306, 1954.

12. Gabe, D. R. and Makanjuola, P. A. “Enhanced Mass Transfer Using Roughened Rotating Cylinder Electrodes in Turbulent Flow”, Journal of Applied Electrochemistry, 17, p. 370, 1987.

13. Bienkowsky, J. , “A Rotating Cylinder Electrode with Surface Roughness”, Honours Thesis, Department of Mechanical Engineering, The University Of Queensland, Brisbane, Australia, 1998.

14. Linton, W. H. and Sherwood, T. K., “Mass Transfer from Solid Shapes to Water in Streamline and Turbulent Flow”, Chemical Engineering Progr., 46, p. 288, 1950.

15. Van Shaw, P., Reiss, L. P. and Hanratty, T. J., “Rates of Turbulent Transfer to a Pipe Wall in the Mass Transfer Entry Region”, Journal of the American Institute of Chemical Engineers, 9, p. 362, 1963.

16. Sydberger, T. and Lotz, U. “Relation Between Mass Transfer and Corrosion in a Turbulent Pipe Flow”, Journal of the Electrochemical Society: Electrochemical Science and Technology, 129, p. 276, 1982.

17. Lezius, D. K. and J. P. Johnston, “Roll-cell instabilities in rotating laminar and turbulent channel flows”, Journal of Fluid Mechanics, 77, p. 153, 1976.

18. Rosenfeld, M., D. Kwak, and M. Vinokur, “A Fractional Step Solution Method for the Unsteady Incompressible Navier-Stokes Equations in Generalized Coordinate Systems”, Journal of Computational Physics, 94, p. 102, 1994.

19. Le, H., P. Moin, and J. Kim, “Direct numerical simulation of turbulent flow over a backward-facing step”, Journal of Fluid Mechanics, 330, p. 349, 1997.

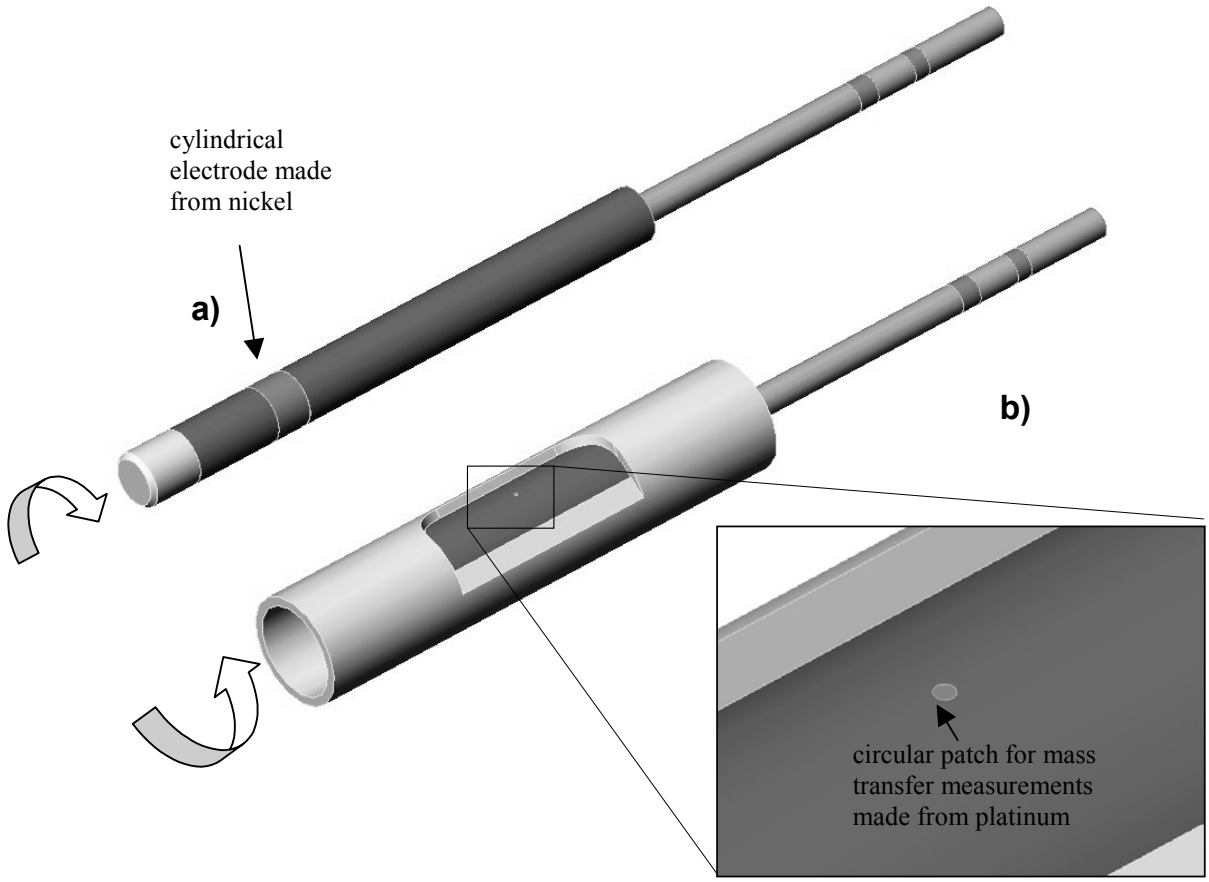

Figure 1. a) A standard rotating cylinder electrode mounted on a shaft.
b) A rotating cylinder electrode with a step.

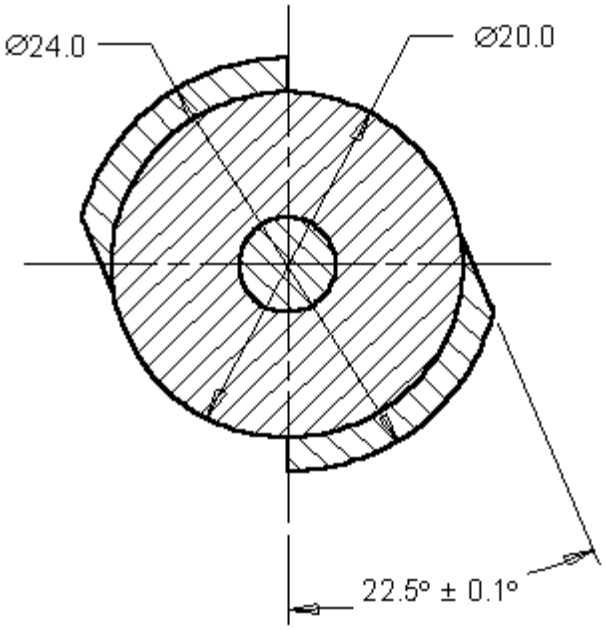

Figure 2. Cross-section of the center section of the rotating cylinder with the two steps.

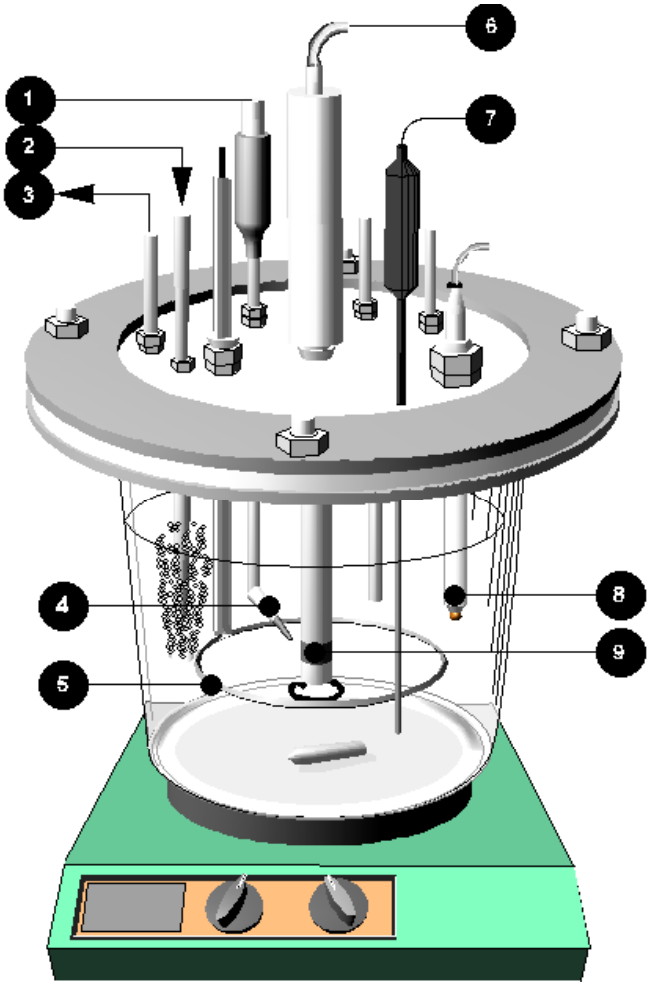

Figure 3. Schematic of a typical experimental test cell: 1-reference electrode, 2-gas in, 3-gas out, 4-Luggin capillary, 5- counter electrode, 6-rotating cylinder, 7-temperature probe, 8-pH electrode, 9-rotating cylinder and probe.

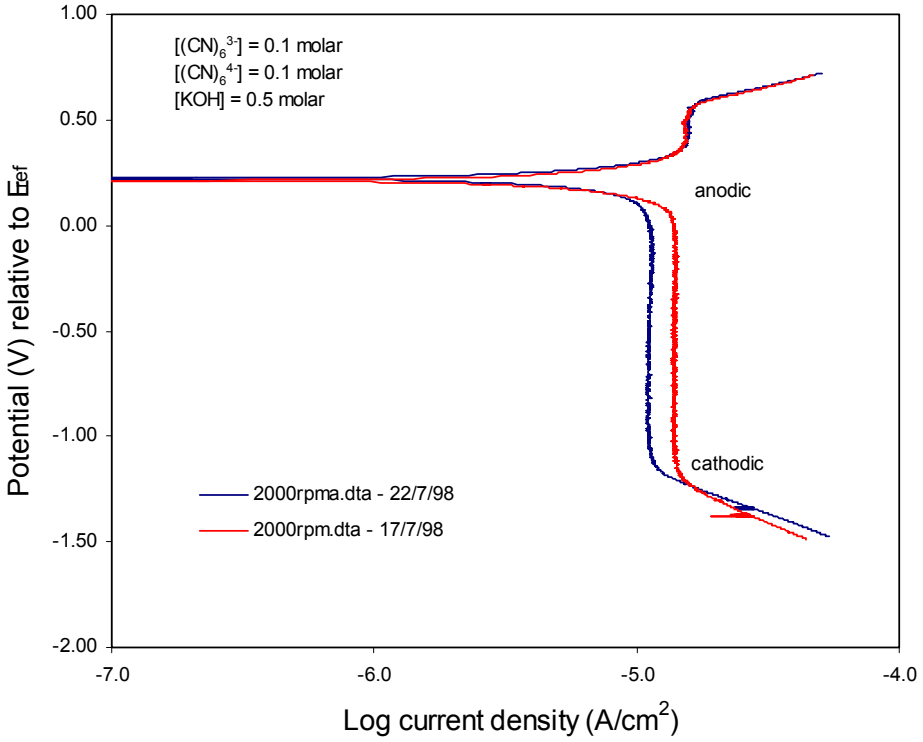

Figure 4. Test of repeatability in experiments with the ferri / ferro cyanide system at 2000 RPM.

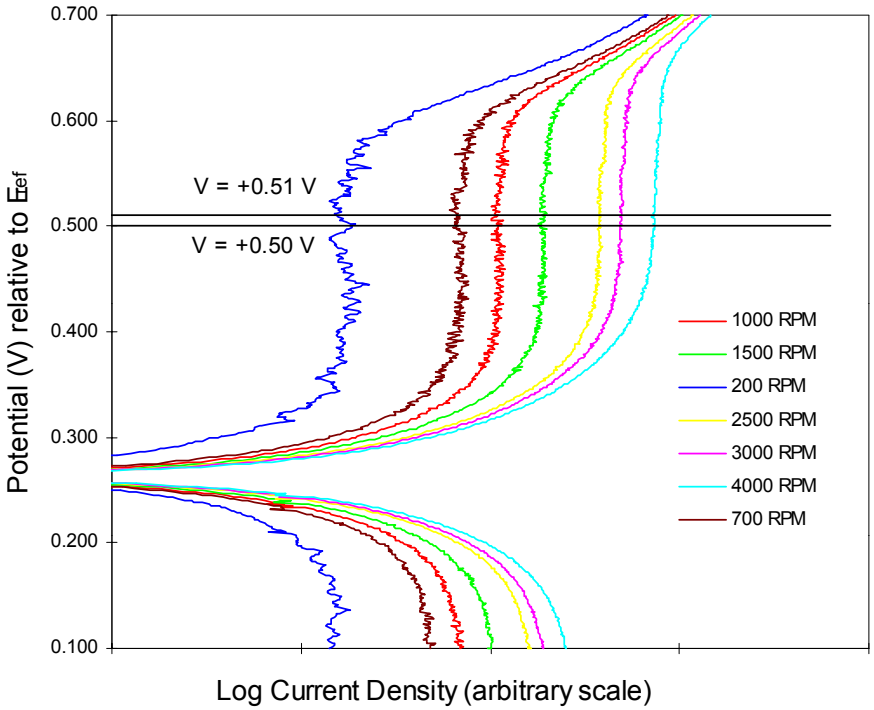

Figure 5. The anodic diffusion limiting current potential window on the rotating cylinder electrode.

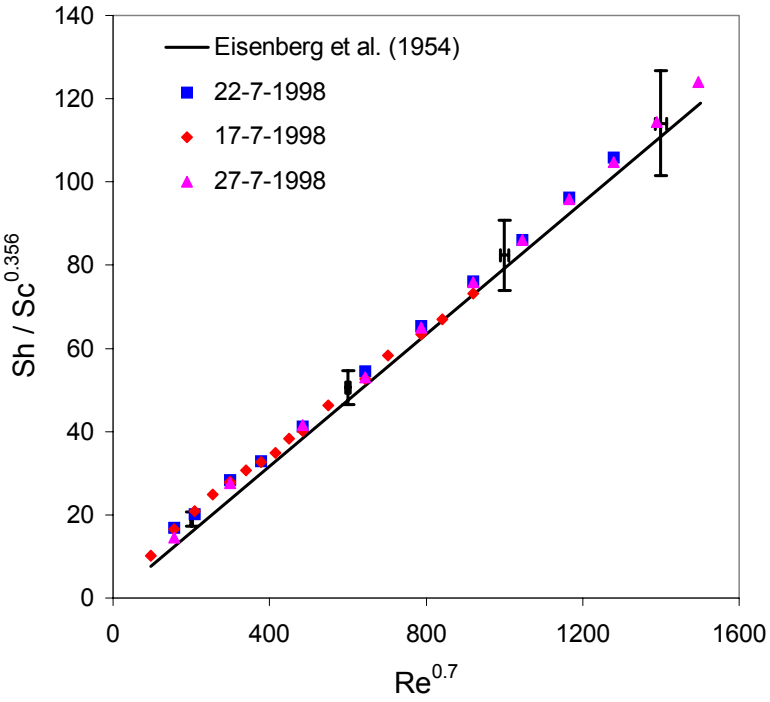

Figure 6. Results of mass transfer measurements using a standard rotating cylinder electrode compared with the Eisenberg et al. [11] correlation.

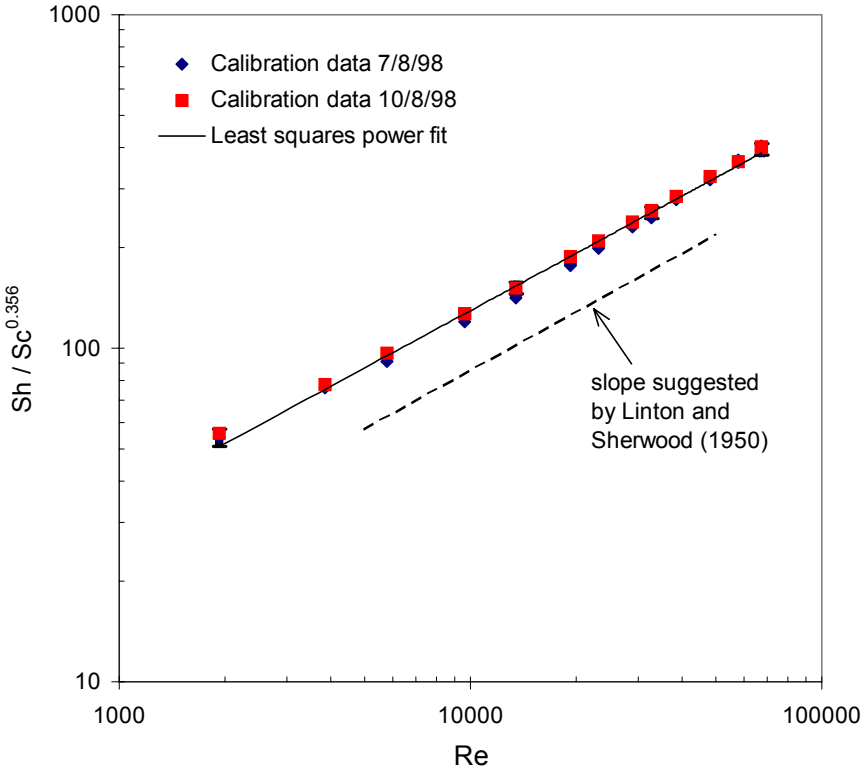

Figure 7. Calibration of the platinum patch electrode obtained using the rotating cylinder geometry without the step.

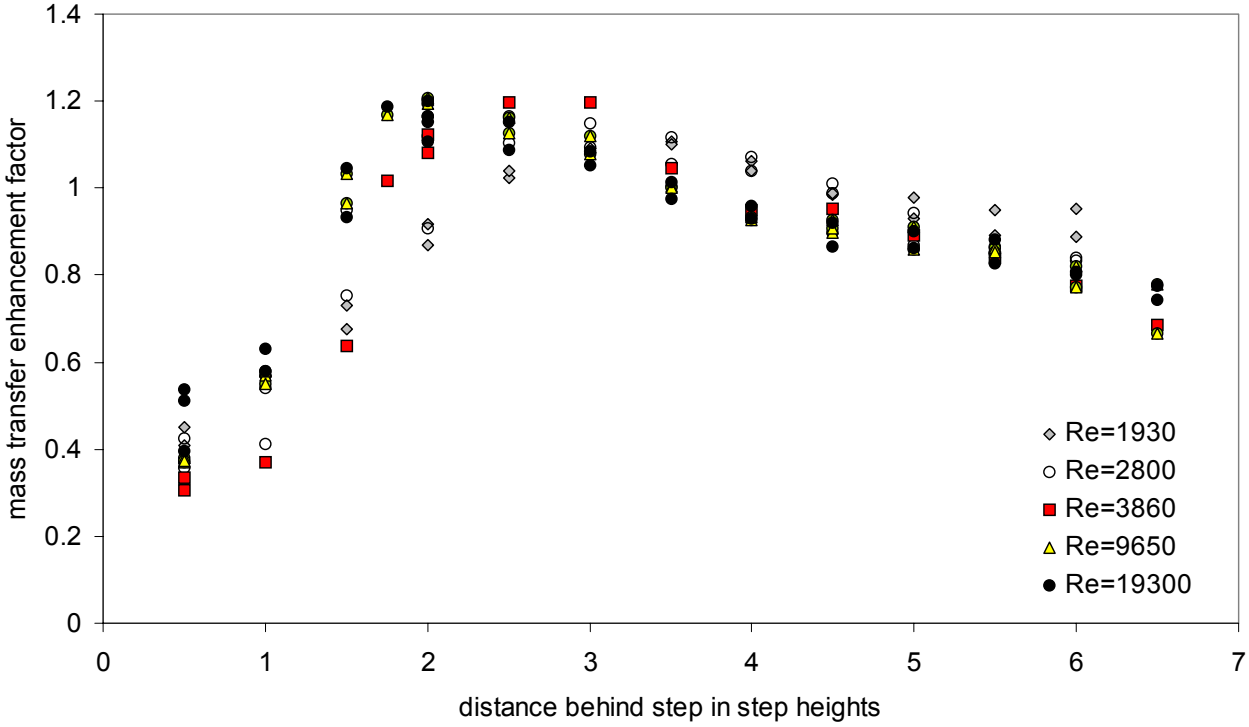

Figure 8. The enhancement of mass transfer behind the step as a function of distance behind the step for a range of Reynolds numbers studied.

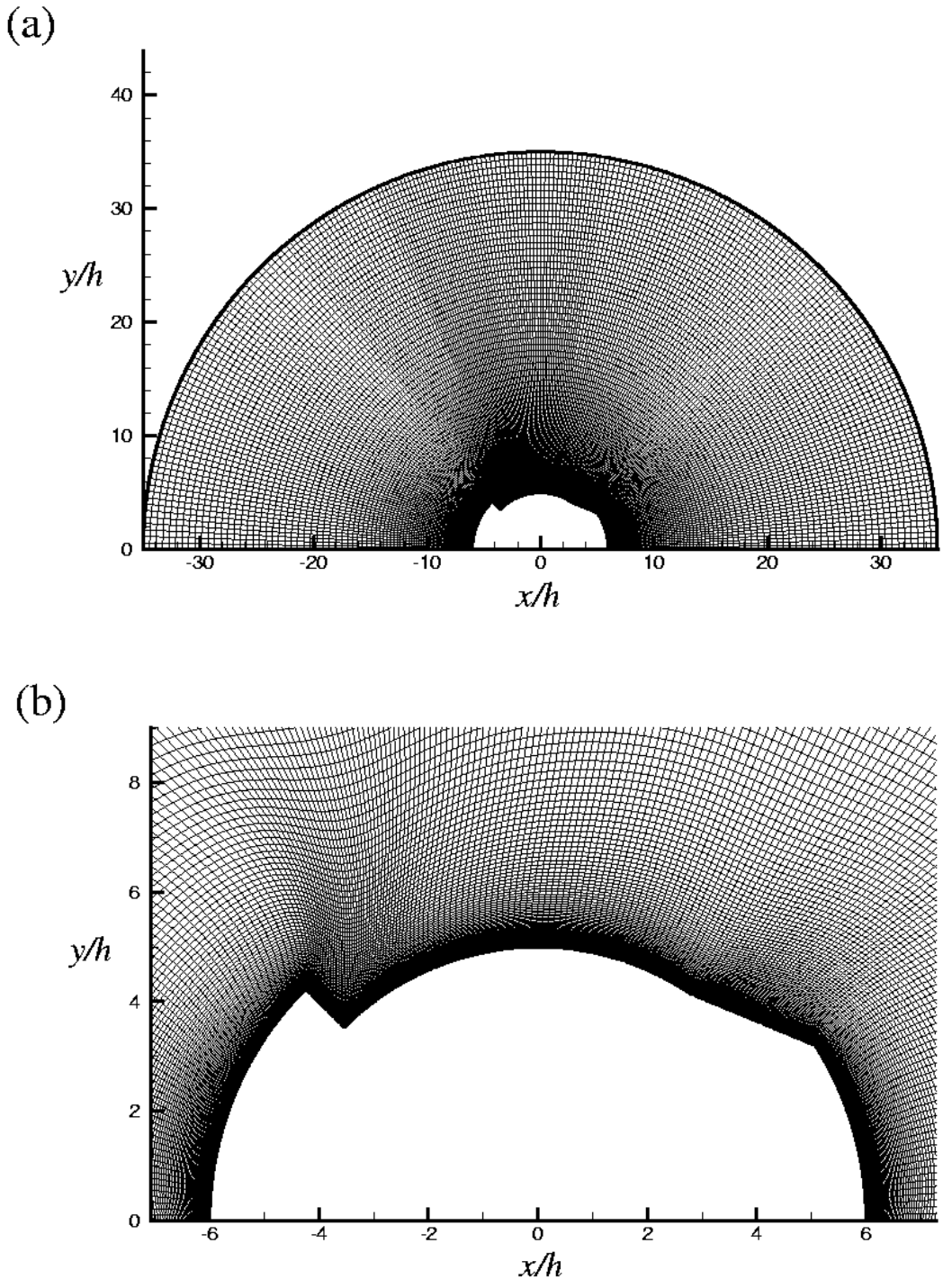

Figure 9. The computational grid.

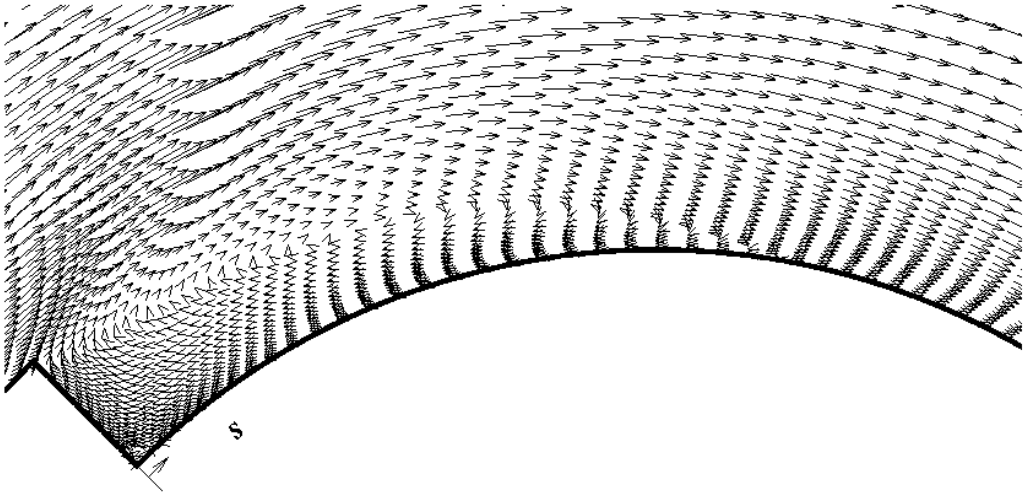

Figure 10. The predicted mean velocity vector plot near the step (averaged in time and the axial direction).

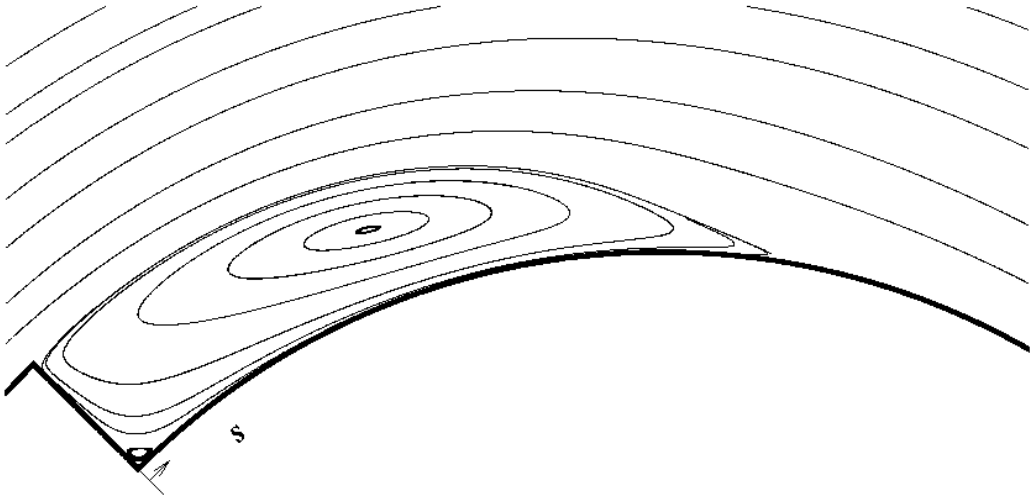

Figure 11. The predicted mean streamlines near the step (averaged in time and the axial direction).

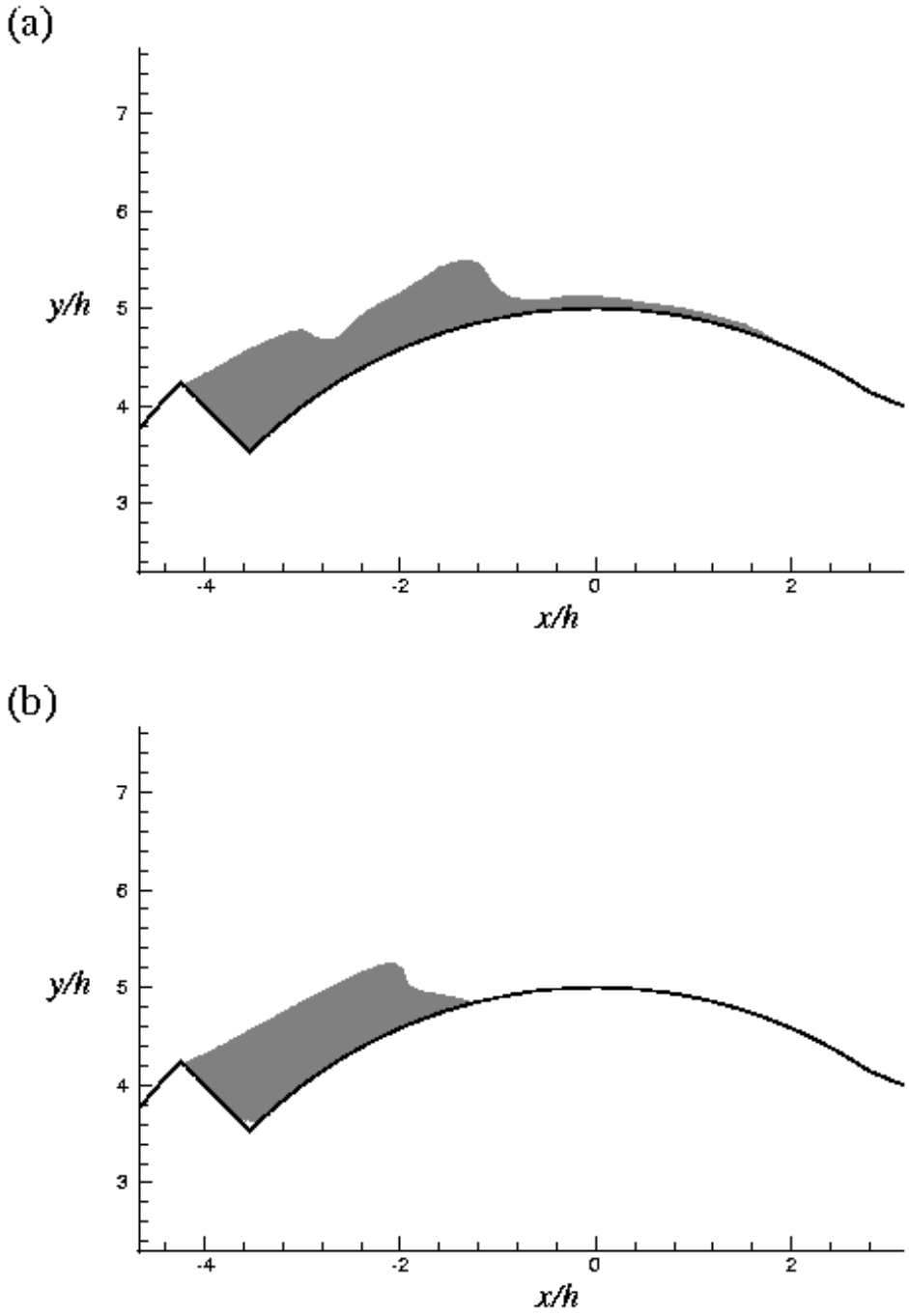

Figure 12. Instantaneous flow pattern (dark colour denoting the region of negative tangential velocity – i.e. reversed flow) at the same axial cross section and at two different times approximately 0.58 revolutions apart.

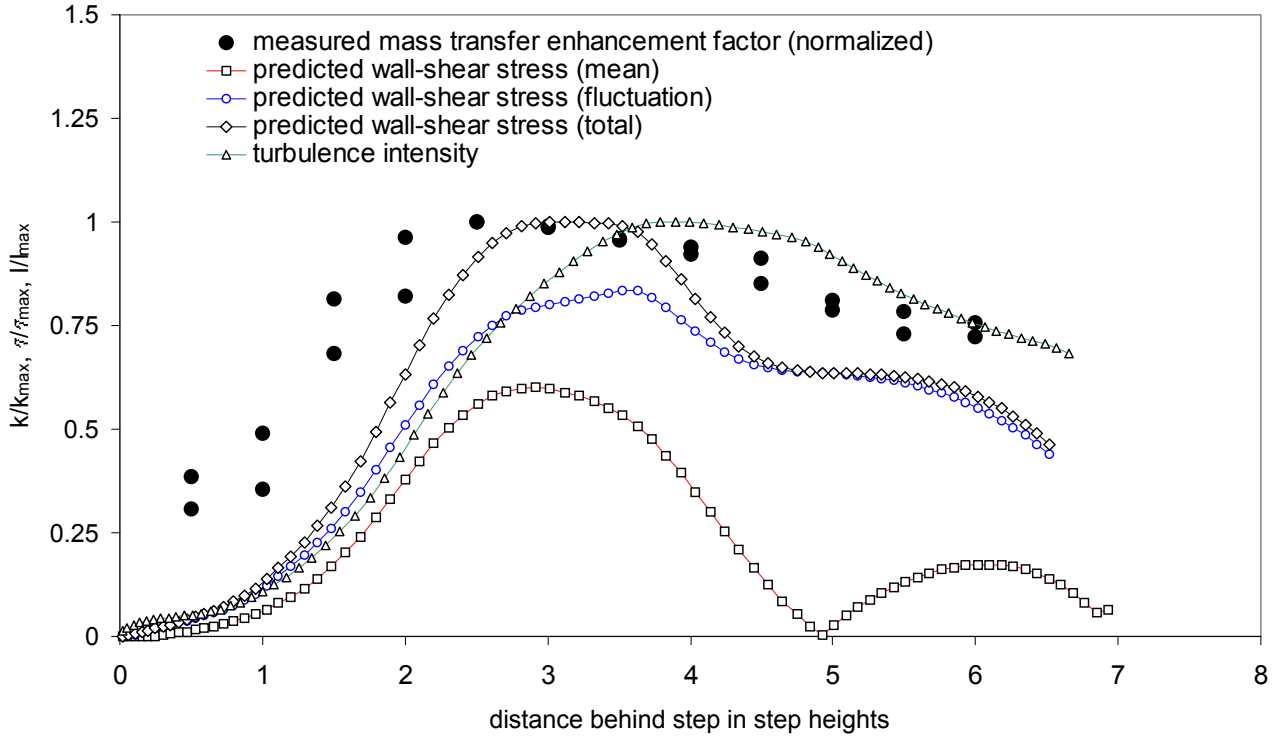

Figure 13. Computed turbulence intensity, mean (time averaged) tangential wall-shear stress, the fluctuating component (rms of its fluctuation) and the sum of the two (total wall-shear stress) compared to the mass transfer enhancement factor as a function of distance behind the step. All the computational values are averaged in time and in the axial direction and normalized with $\frac{1}{2}\rho U_\theta^2$. All values are further normalized with the maximum value for easier comparison. Re=2800.

Figure 1. a) A standard rotating cylinder electrode mounted on a shaft. b) A rotating cylinder electrode with a step.

Figure 2. Cross-section of the center section of the rotating cylinder with the two steps.

Figure 3. Schematic of a typical experimental test cell: 1-reference electrode, 2-gas in, 3-gas out, 4-Luggin capillary, 5- counter electrode, 6-rotating cylinder, 7-temperature probe, 8-pH electrode, 9-rotating cylinder and probe.

Figure 4. Test of repeatability in experiments with the ferri / ferro cyanide system at 2000 RPM.

Figure 5. The anodic diffusion limiting current potential window on the rotating cylinder electrode.

Figure 6. Results of mass transfer measurements using a standard rotating cylinder electrode compared with the Eisenberg et al. [11] correlation.

Figure 7. Calibration of the platinum patch electrode obtained using the rotating cylinder geometry without the step.

Figure 8. The enhancement of mass transfer behind the step as a function of distance behind the step for a range of Reynolds numbers studied.

Figure 9. The computational grid.

Figure 10. The predicted mean velocity vector plot near the step (averaged in time and the axial direction).

Figure 11. The predicted mean streamlines near the step (averaged in time and the axial direction).

Figure 12. Instantaneous flow pattern (dark colour denoting the region of negative tangential velocity – i.e. reversed flow) at the same axial cross section and at two different times approximately 0.58 revolutions apart.

Figure 13. Computed turbulence intensity, mean (time averaged) tangential wall-shear stress, the fluctuating component (rms of its fluctuation) and the sum of the

two (total wall-shear stress) compared to the mass transfer enhancement factor as a function of distance behind the step. All the computational values are averaged in time and in the axial direction and normalized with $\frac{1}{2}\rho U_0^2$. All values are further normalized with the maximum value for easier comparison. Re=2800.